

GRB 080517: A local, low luminosity GRB in a dusty galaxy at $z=0.09$

Elizabeth R. Stanway^{1*}, Andrew J. Levan¹, Nial Tanvir², Klaas Wiersema²,
Alexander van der Horst³, Carole G. Mundell⁴, Cristiano Guidorzi⁵

¹*Department of Physics, University of Warwick, Gibbet Hill Road, Coventry, CV4 7AL, UK*

²*Department of Physics and Astronomy, University of Leicester, University Road, Leicester LE1 7RH, UK*

³*Anton Pannekoek Institute, University of Amsterdam, Science Park 904, 1098 XH Amsterdam, The Netherlands*

⁴*Astrophysics Research Institute, Liverpool John Moores University, IC2, Liverpool Science Park, 146 Brownlow Hill, Liverpool L3 5RF, UK*

⁵*Department of Physics and Earth Sciences, University of Ferrara, via Saragat 1, I-44122, Ferrara, Italy*

Accepted 2014 October 28. Received 2014 October 23; in original form 2014 September 19

ABSTRACT

We present an analysis of the photometry and spectroscopy of the host galaxy of *Swift*-detected GRB 080517. From our optical spectroscopy, we identify a redshift of $z = 0.089 \pm 0.003$, based on strong emission lines, making this a rare example of a very local, low luminosity, long gamma ray burst. The galaxy is detected in the radio with a flux density of $S_{4.5\text{ GHz}} = 0.22 \pm 0.04\text{ mJy}$ - one of relatively few known GRB hosts with a securely measured radio flux. Both optical emission lines and a strong detection at $22\mu\text{m}$ suggest that the host galaxy is forming stars rapidly, with an inferred star formation rate $\sim 16\text{ M}_{\odot}\text{ yr}^{-1}$ and a high dust obscuration ($E(B-V) > 1$, based on sight-lines to the nebular emission regions). The presence of a companion galaxy within a projected distance of 25 kpc, and almost identical in redshift, suggests that star formation may have been triggered by galaxy-galaxy interaction. However, fitting of the remarkably flat spectral energy distribution from the ultraviolet through to the infrared suggests that an older, 500 Myr post-starburst stellar population is present along with the ongoing star formation. We conclude that the host galaxy of GRB 080517 is a valuable addition to the still very small sample of well-studied local gamma-ray burst hosts.

Key words: gamma-ray burst:individual:080517 – galaxies:star formation – galaxies:structure – galaxies: distances and redshifts

1 INTRODUCTION

Long Gamma Ray Bursts (GRBs) are intense, relativistically beamed, bursts of radiation, likely emitted during the collapse of a massive star at the end of its life (Woosley & Heger 2006). As well as constraining the end stages of the evolution for massive stars, they also mark out star formation in the distant Universe, in galaxies often too small to observe directly through their stellar emission or molecular gas (e.g. Tanvir et al. 2012). However, extrapolating from the detection of a single stellar event (the burst) to their wider environment, and the contribution of their hosts to the volume averaged cosmic star formation rate (e.g. Robertson & Ellis 2012), is challenging. Doing so relies on a good understanding of the stellar populations and physical conditions that give rise to GRB events.

This understanding has improved significantly over recent years. A number of studies now constrain the stellar properties of typical GRB hosts (e.g. Savaglio, Glazebrook, & LeBorgne 2009; Svensson et al. 2010; Hjorth et al. 2012), their radio properties (e.g. Michałowski et al. 2012; Stanway, Davies, & Levan 2010; Stanway, Levan, & Davies 2014; Perley et al. 2014) and behaviour in the far-infrared (Hunt et al. 2014; Symeonidis et al. 2014). However these studies have also demonstrated diversity within the population. GRB host galaxies range from low mass, metal poor galaxies forming stars at a moderate rate (e.g. Levesque et al. 2010), to more massive moderately dusty but not extreme (SMG-like) starbursts such as the ‘dark’ burst population (Perley et al. 2013; Perley & Perley 2013).

The challenge of understanding these sources has been complicated by the high redshifts at which they typically occur. The long GRB redshift distribution peaks beyond

* E-mail: e.r.stanway@warwick.ac.uk

$z = 1$ (Jakobsson et al. 2012), tracing both the rise in the volume-averaged star formation rate and the decrease in typical metallicity - which may favour the formation of GRB progenitors (see e.g. Robertson & Ellis 2012, and references therein); local examples which can be studied in detail are rare. Of long duration (>2 s) bursts in the official *Swift Space Telescope* GRB catalogue table¹, only three are listed as having $z < 0.1$. A few other (pre-*Swift*) bursts are also known at low redshifts (e.g. GRB 980425 at $z = 0.009$ Galama et al. 1998), but were detected by instruments with quite different systematics and tend to be unusual systems. One of the most recent studies, which exploited ALMA data, identified the host of GRB 980425 as a dwarf system with low dust content and suggested that this is typical of GRB hosts as a whole (Michałowski et al. 2014). However each low redshift host investigated in detail has informed our understanding of the population as a whole and proven to differ from the others (e.g. Watson et al. 2011; Starling et al. 2011). Low redshift bursts include several which are sub-luminous, such as GRBs 090825 and 031203 (Galama et al. 1998; Malesani et al. 2004; Soderberg et al. 2004), and others such as GRBs 060505 and 060614 that were long bursts without associated supernovae (Fynbo et al. 2006; Della Valle et al. 2006). Cross-correlation with local galaxy surveys (at $z < 0.037$) has suggested that some low redshift GRBs in the existing burst catalogues have yet to be identified as such (Chapman et al. 2007) and hence opportunities to study their properties in detail have been missed. Given the very small sample, and the variation within it, it is important that we continue to follow up the hosts of low redshift bursts and do not allow a few examples to skew our perception of the population.

We have acquired new evidence suggesting that a previously overlooked burst, GRB 080517, and its host galaxy might prove a valuable addition to the study of local gamma ray bursts. The WISE all-sky survey (Wright et al. 2010), publically released in 2012, maps the sky at $3\text{--}22\ \mu\text{m}$. While the observations are relatively shallow and most GRB hosts remain undetected or confused, we have identified the host of GRB 080517 as anomalous. Not only is an infrared-bright source clearly detected coincident with the burst location, but it has a sharply rising spectrum and is extremely luminous in the $22\ \mu\text{m}$ W4 band, suggesting that it is a rather dusty galaxy, and likely at low redshift.

In this paper, we present new photometry and spectroscopy of the host of GRB 080517, identifying its redshift as $z = 0.09$. Compiling archival data, we consider the spectral energy distribution (SED) of the host galaxy, and also its larger scale environment, evaluating the source as a low redshift example of a dusty GRB host galaxy. In section 2 we discuss the initial identification of this GRB and its properties. In section 3 we present new data on the host galaxy of this source. We present our optical photometry and spectroscopy of the GRB host and a neighbouring companion in section 3.2 and report a detection of the GRB host at radio frequencies in section 3.3. In section 4 we reassess the initial burst properties and its early evolution in the light of our new redshift information. In section 5 we compile new and archival photometry to secure an analysis of the spectral en-

ergy distribution, and in section 6 report constraints on the host galaxy's star formation rate. In section 7 we discuss the properties of the host galaxy in the context of other galaxy populations before presenting our conclusions in section 8.

Throughout, magnitudes are presented in the AB system (Oke & Gunn 1983) and fluxes in μJy unless otherwise specified. Where necessary, we use a standard cosmology with $h_0 = 70\ \text{km s}^{-1}\ \text{Mpc}^{-1}$, $\Omega_M = 0.3$ and $\Omega_\Lambda = 0.7$.

2 INITIAL OBSERVATIONS

GRB 080517 triggered the *Swift* Burst Alert Telescope (BAT) at 21:22:51 UT on 17th May 2008 as a flare with a measured T_{90} (i.e. period during which 90% of the burst energy was detected) of 65 ± 27 s, classifying the event as a long GRB. The X-ray Telescope (XRT) identified a fading, uncatalogued point source and the presence of a known optical source was noted within the X-Ray error circle. The final enhanced XRT position, with uncertainty $1''.5$, was 06h 48m 58.03s +50 44 07.7 (J2000), coincident with the optical source (Parsons et al. 2008). The Galactic longitude and latitude ($l = 165.369$, $b = 20.301$) correspond to a sight-line with moderate dust extinction ($A_V = 0.25$) from our own galaxy (Schlafly & Finkbeiner 2011).

Early observations with the Liverpool Telescope, starting 11 minutes after the BAT trigger, did not detect an optical transient outside of the known source (Smith et al. 2008) and no further optical follow-up was undertaken - in part due to the difficult proximity (within 50°) of the Sun at the time the burst triggered *Swift*. Both the lack of an optical afterglow and analysis of the BAT spectrum suggested that the source might lie at high redshifts (Markwardt et al. 2008; Xiao & Schaefer 2011), but constraints on the X-ray spectrum precluded a high redshift fit to the data (Parsons et al. 2008). Association with the known, bright optical source would suggest a lower redshift for the burst, but it was not clear whether this was the host galaxy or a star in chance alignment.

While the afterglow was not detected in the optical, the γ -ray and X-ray emission was also relatively weak, with an early time flux at $0.3\text{--}10\ \text{keV}$ of $2.52^{+1.20}_{-0.75} \times 10^{-10}\ \text{erg cm}^{-2}\ \text{s}^{-1}$, measured in a 10 s exposure at a mean photon arrival time of $T_0 + 133$ s (based on analysis from Evans et al. 2009). In the absence of a redshift for the host, the time-averaged X-ray analysis also suggested the presence of an excess neutral hydrogen column density of $3.0^{+2.1}_{-1.8} \times 10^{21}\ \text{cm}^{-2}$ above the Galactic value of $1.09 \times 10^{21}\ \text{cm}^{-2}$ (where these are 90% confidence intervals in analysis from the UK Swift Science Data Centre, Evans et al. 2009). This represents an excess in the X-ray inferred hydrogen column at the $\sim 3\sigma$ level. *Swift* observations ended approximately 20 hours after the initial trigger.

Initial observations for this source were therefore ambiguous, with different elements of the data either suggesting a high redshift solution (non-detection of the optical transient, BAT spectrum) or appearing to preclude it (optical source association, X-ray spectrum), and the excess extinction seen in the afterglow implying the presence of dust either in the host galaxy or along the line of sight. However the burst's location, within 50° of the Sun at the time the burst went off, precluded further early time studies, and the

¹ http://swift.gsfc.nasa.gov/archive/grb_table/

burst has largely been ignored since. *Swift* has not observed this location at any other time.

Given the presence of a relatively bright, $r_{AB} = 17.73$, catalogued source within the *Swift* XRT error circle, an obvious question arises: what is the probability that this is a chance alignment rather than a genuine host galaxy identification? Two main factors contribute to this determination. The surface density of galaxies observable at a given magnitude will depend both on the properties of the galaxy population with redshift, and with galactic latitude (which will govern the fraction of the sky affected by foregrounds and crowding). To evaluate this, we have studied the galaxy population in regions of the Sloan Digital Sky Survey Data Release 10 (SDSS DR10, Ahn et al. 2014) at comparable Galactic latitude (within $\sim 5^\circ$) and offset by $30\text{--}50^\circ$ in Galactic longitude. The population identified by the SDSS photometric pipeline as galaxies were selected in ten regions, each with a diameter of 1° , and their surface density evaluated as a function of r' -band magnitude.

As figure 1 illustrates, the surface density of galaxies comparable to the proposed host of GRB 080517 is low, with 0.028 ± 0.006 galaxies typically found per square arcminute. Assuming that the SDSS photometric classification is accurate, the probability of finding a galaxy of this brightness within 3 arcseconds (see figure 2) of a given X-ray location is just 0.007%. Taking into account the 604 long bursts with X-ray localisations in the *Swift Space Telescope* GRB catalogue table, we would expect 0.04 chance alignments amongst the entire long GRB population.

A further constraint arises from the nature of the GRB itself. GRB 080517 was a long burst, believed to be associated with a core collapse progenitor, and so likely to be associated with recent or ongoing star formation. If we consider only those galaxies in SDSS with the flat optical colours associated with ongoing star formation, i.e. $|r' - i'| < 0.5$, the surface density of galaxies drops still further, to just 0.021 ± 0.006 galaxies per square arc minute, and a predicted 0.03 chance alignments in the entire GRB sample.

As will be discussed below, the possible host galaxy of GRB 080517 is strongly star forming, and lies within 3 arcseconds of the burst location. Thus we propose its identification as the burst host.

3 FOLLOW-UP DATA

3.1 WHT Imaging

We targetted the host of GRB 080517 on the night of 2014 Feb 25 (i.e. 6 years post-burst) using the auxiliary-port camera, ACAM, on the William Herschel Telescope (WHT). Photometric imaging was acquired in the Sloan g , r and i bands, with an integration time of 180s in each band. Observations were carried out as part of programme W/2014/9 (PI: Levan) and photometric data were reduced and calibrated using standard IRAF procedures.

As figure 2 demonstrates, the 1.2 arcsecond seeing was sufficient to determine the morphology of both the host galaxy and a near neighbour, separated from it by 16 arcseconds. While the GRB host shows a relatively smooth, relaxed morphology, it is resolved in our imaging with a measured gaussian FWHM of 2.1 arcseconds. Deconvolution

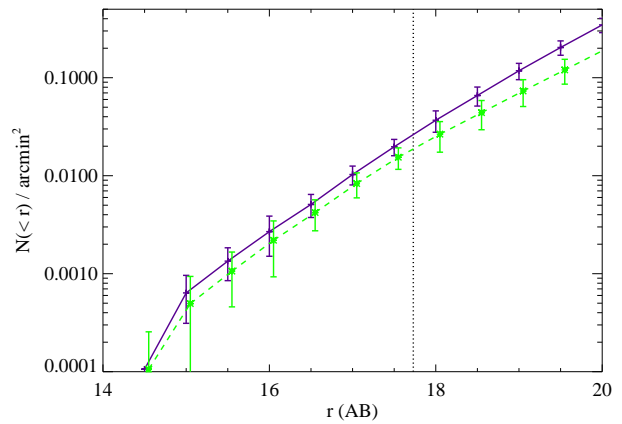


Figure 1. The surface density of galaxies brighter than a given r' -band magnitude, at comparable galactic latitude to GRB 080517, based on photometric classification in the Sloan Digital Sky Survey. The solid line shows the surface density of all galaxies, with the standard deviation measured across ten 1° -diameter fields. The dashed line shows the lower surface density of relatively blue galaxies likely to be star-forming. The dotted vertical line indicates the magnitude of the proposed host of GRB 080517.

with the seeing, as measured from unresolved sources in the image, yields an estimated intrinsic size of 1.6 arcseconds, or 2.7 kpc at $z = 0.09$ (see next section).

While we are unable to distinguish clumpiness on sub-kiloparsec scales, the host galaxy is sufficiently resolved in this new imaging to place constraints on its radial light profile, although such constraints are necessarily limited by the relatively large (0.253 arcsecond) pixels relative to the seeing. In figures 3 and 4 we compare the radially averaged light profile of the galaxy with Sersic profiles (see Graham & Driver 2005, for definitions and discussion), which have been convolved with the seeing in the image. It is clear that a de Vaucouleurs law ($n = 4$), such as describes local giant elliptical galaxies would predict far too steep a light profile. Allowing the effective radius and Sersic parameter to vary simultaneously, the best fit to the data is found for $n = 1.5 \pm 1.0$ and $R_e = 1.7 \pm 0.8''$.

3.2 WHT Spectroscopy

We also obtained spectroscopic data from ACAM on the same night, using the V400 grating and a total integration time of 4×600 s, producing a spectrum spanning $4000\text{--}9000\text{\AA}$ with a spectral resolution measured from unblended arc lines of $\sim 18\text{\AA}$ ($\sim 1000\text{ km s}^{-1}$). Both photometric and spectroscopic data were reduced and calibrated using standard IRAF procedures. Absolute flux and wavelength calibration were achieved through observations of a standard star field and arc lamps immediately preceding the science data.

The slit was oriented at a position angle of 50° , so as to pass through the centres both of the GRB host and the bright neighbour, separated from it by $16''$ measured along the $1''.5$ slit.

Both the GRB host galaxy and its neighbour are detected at high signal to noise in our spectroscopy. The latter

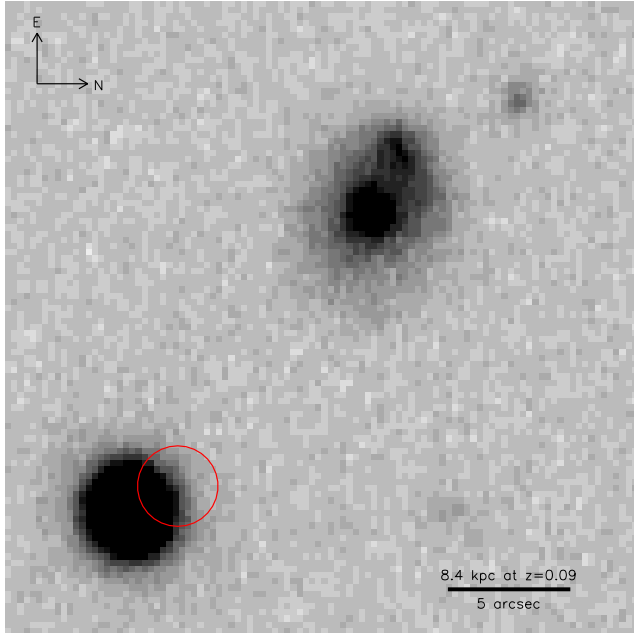


Figure 2. The structure of the compact GRB host galaxy (lower left) and its near-neighbour (upper right) in the Sloan-*i* band from our WHT imaging. The neighbour clearly has two cores within a more diffuse galaxy, and is likely to be undergoing a major merger. Both sources are at the same redshift (see section 3.2), the scale bar indicates physical distance at this redshift. The 1.5 arcsecond 90% confidence error circle from the *Swift* XRT detection of the burst is indicated in red.

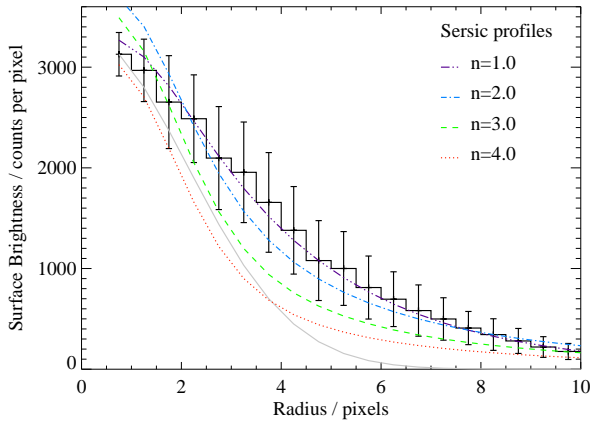


Figure 3. The radial surface brightness profile of the GRB host galaxy in the Sloan-*i* band from our WHT imaging. Sersic profiles have been convolved with the seeing and overplotted for comparison. Given the large error bars - due to compact morphology relative to the pixel scale and seeing - a range of Sersic parameters provide a reasonable fit to the data. Normalising the profiles close to the centre suggests a Sersic index of $n \sim 1.0 - 2.0$ may provide the best description of this galaxy's light profile. The gaussian seeing is shown as a solid line for comparison.

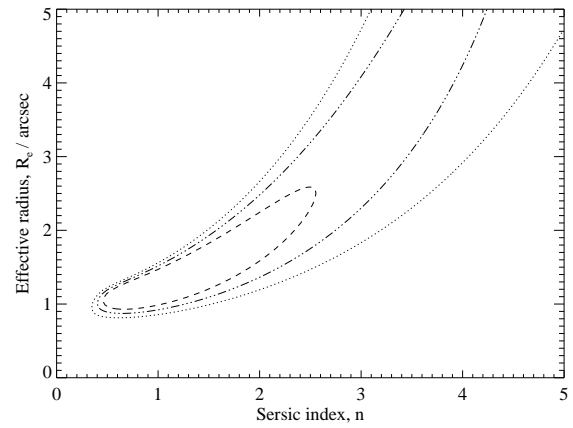


Figure 4. The allowed regions of parameter space for a Sersic light profile, quantified by χ^2 -fitting against the data. Small effective radii ($< 2''$) and low Sersic indices ($n \sim 1-2$) are favoured by the data, but there are substantial degeneracies between these parameters. Contours are shown at 1, 2 and 3 σ confidence levels.

clearly shows two components, A and B. Of these, component A is the stronger continuum source, while component B appears to show relatively stronger line emission (see figure 5). In table 1 we provide the relative emission line strengths of each source (also shown graphically in figure 6). Line equivalent widths are presented in the observed frame. We make no adjustment for slit losses since it is difficult to reconstruct precisely where on the object the 1.5 arcsec wide slit was placed, and harder still to estimate whether line ratios in the regions of the galaxy outside the slit are comparable to those in observed regions. The measured redshift for the host galaxy is $z = 0.089 \pm 0.003$ and for the neighbour $z = 0.091 \pm 0.003$ (for both components). The uncertainty, estimated by cross correlation against a template starburst spectrum, comprises instrumental resolution effects, the effects of blending on many of the lines and uncertainty due to small shifts in velocity offset between different emission lines.

While we adopt the cross-correlation redshifts and conservative associated uncertainties for our analysis, we also consider the redshift derived from the observed wavelength of individual emission lines. Fitting gaussian profiles to the unblended H β and [O III] and the strong, but somewhat blended H α lines, we derive redshifts $z = 0.0903 \pm 0.0006$, 0.0925 ± 0.0006 and 0.0930 ± 0.0003 for the GRB host and components A and B of the companion respectively, where the error now represents the scatter between individual line centroids on each source rather than including other uncertainties. These imply velocity offsets of $\Delta v = 150 \pm 155 \text{ km s}^{-1}$ (i.e. no significant offset) between the two components of the companion and $\Delta v = 576 \pm 155 \text{ km s}^{-1}$ between the host and the companion.

This velocity offset places the galaxy pair just outside (although within one standard deviation of) the criteria used to select galaxy pairs in the SDSS by Ellison et al. (2008), who placed a cutoff for their sample at $\Delta v = 500 \text{ km s}^{-1}$. Those authors recognise however that this cutoff requires a trade-off between contamination and completeness, with

Line	Host	Neighbour A	B
[O II]3726	61.9 \pm 8.0		
[O II]3729	31.0 \pm 4.0		
H γ	6.5 \pm 0.4		
H β	16.8 \pm 1.0	3.2 \pm 1.3	22 \pm 9
[O III]4959	5.8 \pm 0.3	4.1 \pm 1.7	27 \pm 11
[O III]5007	17.1 \pm 1.0	12.4 \pm 5.0	77 \pm 32
He I 5875	2.8 \pm 0.1		
[O I]6300	6.1 \pm 0.2		
[N II]6548	10.3 \pm 0.2	1.6 \pm 0.1	4.1 \pm 0.4
H α	103.1 \pm 2.4	31.8 \pm 1.5	116 \pm 12
[N II]6583	31.5 \pm 0.7	4.9 \pm 0.2	12.5 \pm 1.2
[S II]6716	13.3 \pm 0.5		
[S II]6730	13.0 \pm 0.5		

Table 1. Line strengths measured for the target objects. All measures are given as observed-frame equivalent widths in Angstroms. Measurement of weak lines is not attempted in the fainter neighbour, and it is impossible to isolate the two components in the [O II] line.

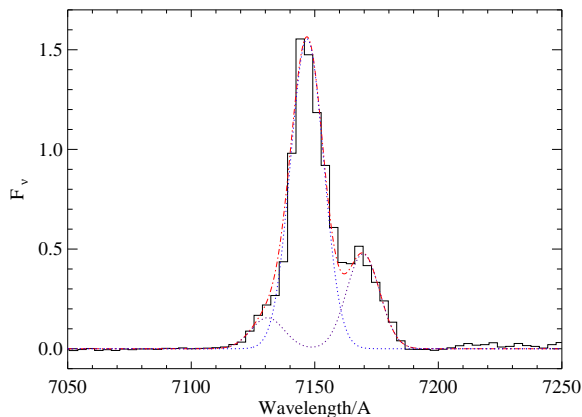


Figure 7. The spectral region containing H α and the [N II] doublet. All three lines are consistent with the being unresolved at the instrumental FWHM. The relative strength of the doublet lines is consistent with that predicted from the electron transition probabilities.

genuine pairs observed out to $\Delta v \sim 600 \text{ km s}^{-1}$ separations (Ellison et al. 2008; Patton et al. 2000). Ellison et al. (2008) identified an enhancement in star formation rate for pairs with projected separations $< 30 - 40 \text{ kpc}$, a criterion easily satisfied by the companion in this case ($16''$ represents $\sim 27 \text{ kpc}$ at this redshift), suggesting that the star formation observed in both host and companion is likely influenced by their proximity.

In figures 7 and 8, we present the spectral regions in the GRB host galaxy associated with line ratios used to classify an ionising spectrum (see section 7). At this spectral resolution, H α is blended with the [N II] doublet, and a fit to the three lines must be obtained simultaneously in order to measure their line strengths. With the exception of close doublets (i.e. [O II], [S II]) the other lines in the spectrum are all comparatively unblended, and all lines are consistent with being essentially unresolved at the instrumental resolution.

The relative intensity of the nebular emission in hydrogen Balmer lines allows us to make an estimate of the

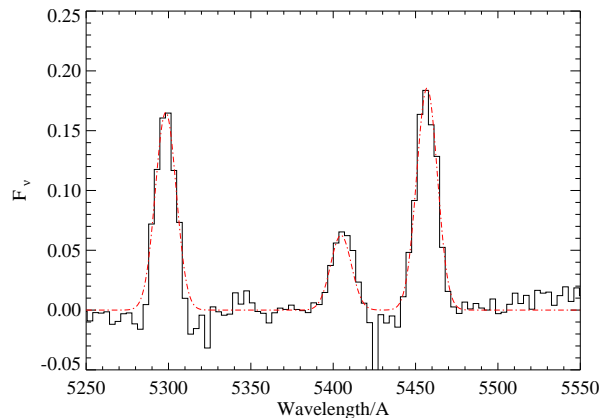


Figure 8. The spectral region containing H β and the [O III] doublet.

dust extinction in the actively star forming region of the GRB host galaxy. The flux in H α is expected to scale relative to H β by a ratio determined by the temperature and electron density of the emitting region. Standard assumptions for these parameters in HII regions ($T=10,000 \text{ K}$, low density limit) yields the widely applied expected ratio of 2.87 (see Osterbrock & Ferland 2006). In figure 9, we scale the line fluxes from the GRB host galaxy accordingly, such that, for Case B reionisation, we would expect each line to have the same relative intensity as H β . It is clear that the Balmer series shows a decrement in the later lines, most likely attributable to dust. Given a Calzetti-like dust law ($R_V = 4.05$, Calzetti et al. 2000), the measured H α /H β ratio implies an extinction of flux from the nebular emission region of the GRB host galaxy of $E(B - V)=1.2$.

Of course, uncertainty arises in whether the HII region parameters and extinction law adopted are indeed appropriate for GRB hosts galaxies. Wiersema (2011) explored a grid of temperatures and dust extinction laws for fitting the H I Balmer series in example spectra and suggested that in the case of the GRB 060218 host a higher temperature and steeper extinction law ($T=15,000 \text{ K}$, $R_V = 4.5$) might be appropriate, while the host of GRB 100316D is best fit with $T \sim 7500 \text{ K}$ and $R_V = 3.5$. The Calzetti dust law lies between that inferred from these two examples, as does our adopted temperature. More detailed spectroscopy (with fainter Balmer lines, and ideally also the He II recombination series) would be required to reach a tighter constraint.

We also obtain a tentative spectroscopic redshift for an unrelated galaxy falling on the long slit. The galaxy, located at RA and Declination $06^h 48^m 59.756^s +50^\circ 44' 23.50''$ (J2000), lies at $z = 0.56$, based on identification of an emission feature as the [O II] 3727Å doublet.

3.3 Radio Observations

The low redshift confirmed for this GRB host makes it an ideal candidate for radio observation. The majority of radio observations of GRB hosts to date have resulted in non-detections, implying star formation rates that do not significantly exceed their UV-optical estimates (e.g.

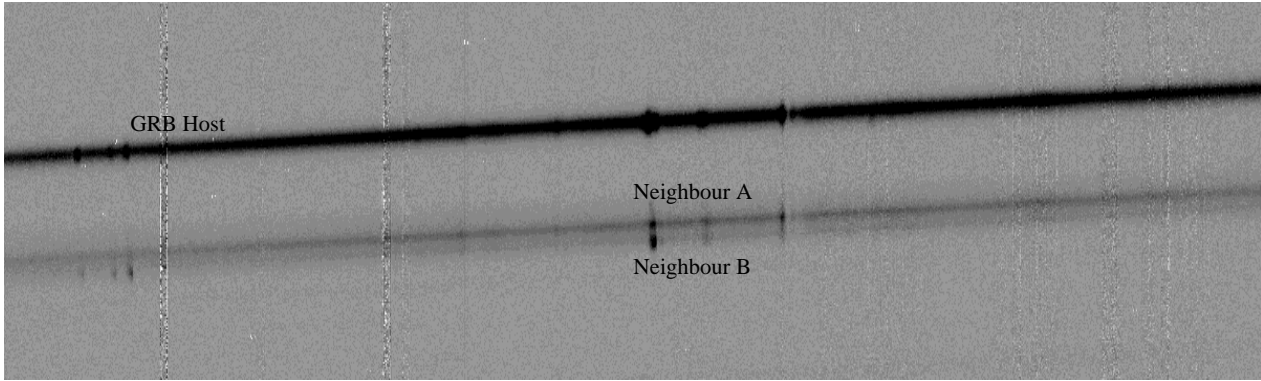


Figure 5. Two dimensional spectrum observed for the GRB host galaxy (at top of the slit) and its neighbour, which divides into two components - A and B. All three components are strong optical line emitters, detected in multiple lines, at the same redshift to within the instrumental resolution. Spectra are aligned such that wavelength increases linearly towards the right of the frame.

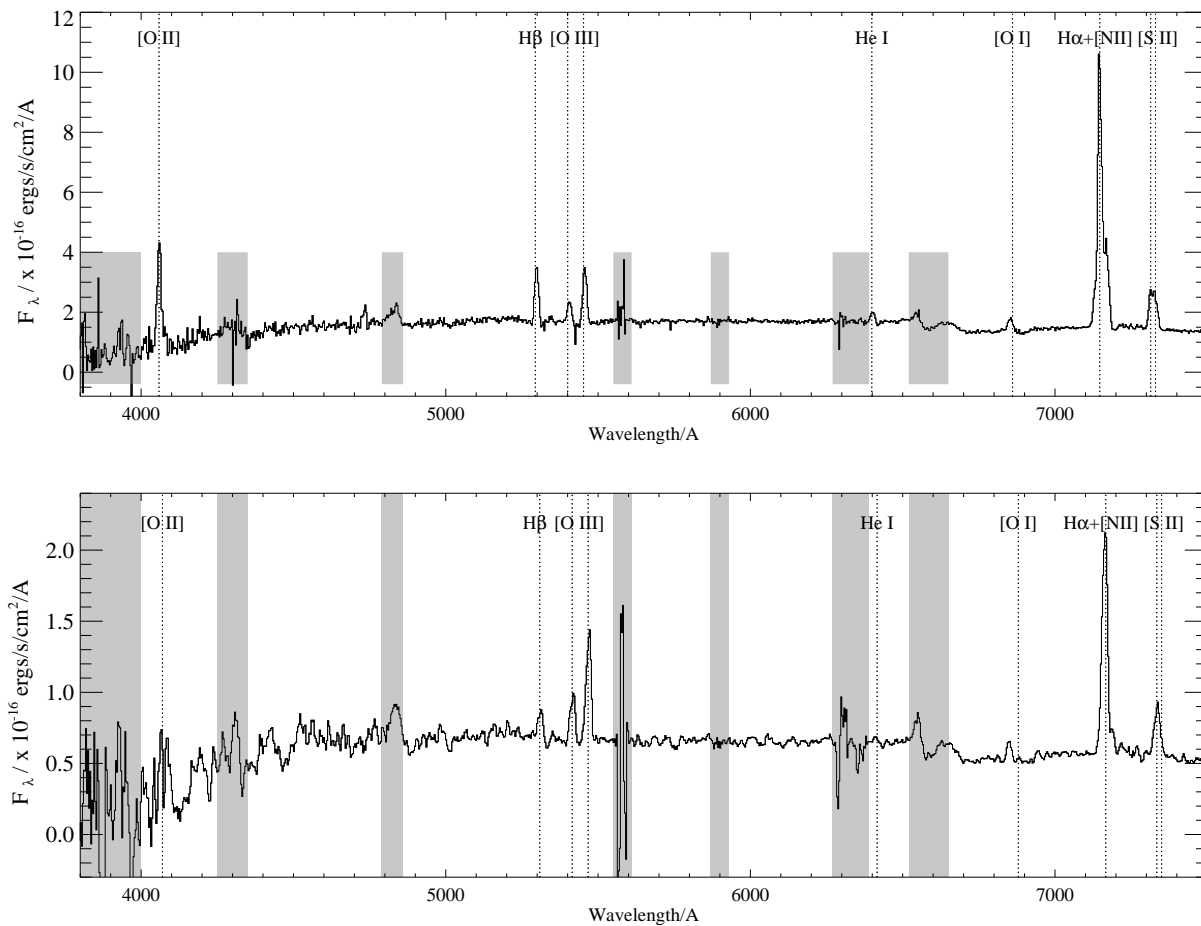


Figure 6. The optical spectra of both the GRB host galaxy (upper plot) and its neighbour (lower). Both sources show strong line emission, well detected continuum flux, and some evidence for a 4000Å break. Wavelengths corresponding to [S II], [N II], H α , O I, He I, [O III], H β and [O II] are indicated. Regions with relatively high noise caused by sky emission line subtraction residuals are indicated by shaded boxes.

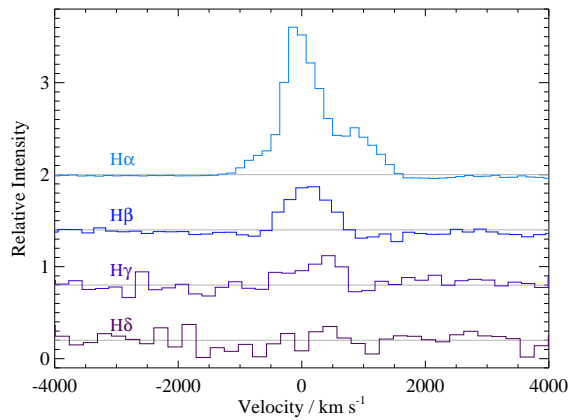


Figure 9. A comparison of the Balmer series emission lines in the GRB host galaxy, scaled by the appropriate line ratios for Case B H I recombination ($T=10^4$ K, low density, Osterbrock & Ferland 2006), such that in the absence of dust, all peaks would be expected to match H β in intensity. The line intensities are offset from zero for clarity. Even accounting for blending with the [N II] doublet, H α still shows a relative excess, consistent with the blue-wards lines being attenuated by a dusty line of sight.

Michałowski et al. 2012; Stanway, Davies, & Levan 2010; Stanway, Levan, & Davies 2014). However, some fraction of GRB hosts appear to be luminous in the submillimetre-radio (Berger et al. 2003; Tanvir et al. 2004), particularly amongst those that show evidence for strong dust extinction (i.e. dark bursts, Perley & Perley 2013; Perley et al. 2014).

Radio observations of the GRB 080517 host galaxy were performed with the Westerbork Synthesis Radio Telescope (WSRT) at 4.8 GHz on 2014 May 2 and May 3 UT, i.e. almost 6 years after the gamma-ray trigger. We used the Multi Frequency Front Ends (Tan 1991) in combination with the IVC+DZB back end in continuum mode, with a bandwidth of 8x20 MHz. Gain and phase calibrations were performed with the calibrator 3C 147. The data were analyzed using the Multichannel Image Reconstruction Image Analysis and Display (MIRIAD; Sault et al. 1995) package.

Both observations resulted in a detection of a source at the position of GRB 080517, with consistent flux densities. We have measured the flux density in an image of the combined data set as $S_{4.8\text{ GHz}} = 0.22 \pm 0.04$ mJy. The detection is consistent with a point source, in observations with a synthesised beam of $14.2 \times 5.3''$ as shown in figure 10. No significant detection is made of the neighbour galaxy - somewhat surprisingly given its high inferred star formation rate (based on H α emission, see section 7).

4 REASSESSING GRB 080517

Given the identification of a redshift for the host galaxy of GRB 080517, we are able to reassess the properties of the burst and its immediate afterglow in the context of an accurate distance (and thus luminosity) measurement, allowing for more meaningful comparison with the rest of the GRB population.

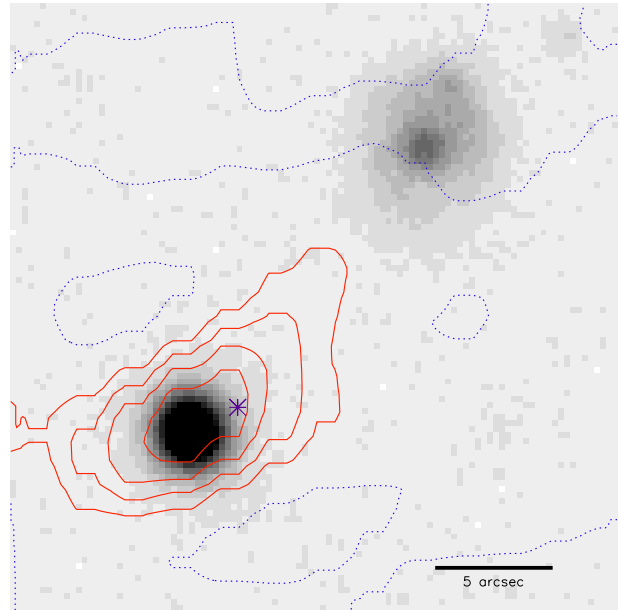


Figure 10. The 4.8 GHz radio flux measured at the WSRT (contours), overlaying the compact GRB host galaxy (lower left) and its near-neighbour (upper right) in the Sloan- r band (greyscale). The contours indicate levels of zero flux (dotted) and $+2, 3, 4$ and 5σ . There are no signals below -2σ in this region. The burst location is indicated with a cross.

4.1 Burst properties

At $z = 0.09$ the inferred isotropic equivalent energy of GRB 080517 is only $E_{iso} = (1.03 \pm 0.21) \times 10^{49}$ ergs, while its 10 hour X-ray luminosity is $L_X \sim 10^{42}$ ergs s^{-1} . Both of these values lie orders of magnitude below the expectations for most GRBs, which have characteristic values of $E_{iso} \sim 10^{52-54}$ ergs (Kocevski & Butler 2008; Cenko et al. 2009) and $L_X \sim 10^{45-47}$ ergs s^{-1} (Nousek et al. 2006). These properties mark GRB 080517 as a member of the observationally rare population of low luminosity GRBs (LL-GRBs). Only a handful of such low luminosity events have been identified in the past decade, all of which have been relatively local (given the difficulty in observing low luminosity bursts beyond $z \sim 0.1$). These include the well studied GRB-supernova pairs GRB 980425/SN 1998bw (Galama et al. 1998), GRB 031203/SN 2003lw (Malesani et al. 2004; Soderberg et al. 2004), GRB 060218/SN 2006aj (Pian et al. 2006) and GRB 100316D/SN 2010bh (Starling et al. 2011; Cano et al. 2011), and the enigmatic GRBs 060505 and 060614, where associated SNe have been ruled out to deep limits, and whose origin remains mysterious (Fynbo et al. 2006; Della Valle et al. 2006). They may be low luminosity events akin to those above, but where the SNe is absent (e.g. Gal-Yam et al. 2006), or they could be GRBs with a similar physical origin to the short-GRBs (most likely NS-NS mergers based on recent observations, Gehrels et al. 2006; Tanvir et al. 2013), in which case their luminosities would be more typical of their population. GRB 080517 adds a further example to these local, low luminosity events. Its highly star forming host galaxy (as discussed later) is perhaps most in keeping with the expectations of long-GRBs, although its

high stellar mass and metallicity would be unusual at such low redshift (Graham & Fruchter 2013).

The prompt emission from GRB 080517, as reported by the *Swift*/BAT instrument, shows a single ‘fast rise, exponential decay’ (FRED Fishman 1995) lightcurve, albeit at low signal to noise. In this respect, its profile is similar to that of low luminosity GRBs 031203 and 980425 (Kaneko et al. 2007), although the profile is not unusual amongst GRBs more generally (Fenimore, Madras, & Nayakshin 1996).

Interestingly, within the low luminosity population there appears to be a good deal of internal diversity. The *Swift*-identified low luminosity events to date – GRB 060218 (Campana et al. 2006) and GRB 100316D (Starling et al. 2011) – appear to be of extremely long duration (2000 s in the case of GRB 060218) with extremely smooth light curves. They are also very soft events in which the X-ray emission exceeds that in the γ -ray (so called X-ray Flashes). In contrast, the pre-*Swift* events (GRB 980425 and GRB 031203) appear to be much closer in prompt properties to classical GRBs, exhibiting shorter durations (tens of seconds) and relatively hard γ -ray spectra. Although there has been some suggestions that GRB 031203 was a softer X-ray event, integrated over longer time periods, this is based on inferences from its X-ray echo (Vaughan et al. 2004), and favour a soft component arising after the initial burst (Watson et al. 2004). In retrospect this is most likely an X-ray flare, as are commonly seen in *Swift* X-ray afterglows (Watson et al. 2006; Nousek et al. 2006). Hence we consider the E_p measured via *INTEGRAL* as likely indicative of the true burst E_p (Sazonov, Lutovinov, & Sunyaev 2004). In this case, both GRB 980425 and GRB 031203 lie well away from the correlation between the peak of the νF_ν spectrum (E_p) and E_{iso} (Amati et al. 2002; Amati 2006).

GRB 080517 appears to have much more in common with these pre-*Swift* events, with a $T_{90} = 65 \pm 27$ s and a hard photon index of $\Gamma \sim 1.5$. While E_p is difficult to directly constrain with the limited BAT bandpass, the Bayesian method of Butler & Kocevski (2007) suggests that $E_p > 55$ keV, making GRB 080517 a significant outlier in the $E_p - E_{iso}$ relation, with a similar location to GRB 980425 and GRB 031203 (see figure 11). Its recovery, some 6 years after the initial detection implies that other, similar, low luminosity events may be present within the *Swift* catalog, since a significant number of bursts have not been followed in depth due to observational constraints. However, GRB 080517 was unusual in having a bright catalogued source within its error box – a relatively rare occurrence. In this context, it should be noted that the host of GRB 080517 is relatively luminous for a GRB host. By contrast, the hosts of GRB 980425 and GRB 060218 would have had observed magnitudes of $r \approx 20$ and $r \approx 22.5$ at $z = 0.1$ and so would not be readily catalogued in DSS and similar survey observations, suggesting that the presence of a catalogued source is not necessarily a good indicator of event frequency.

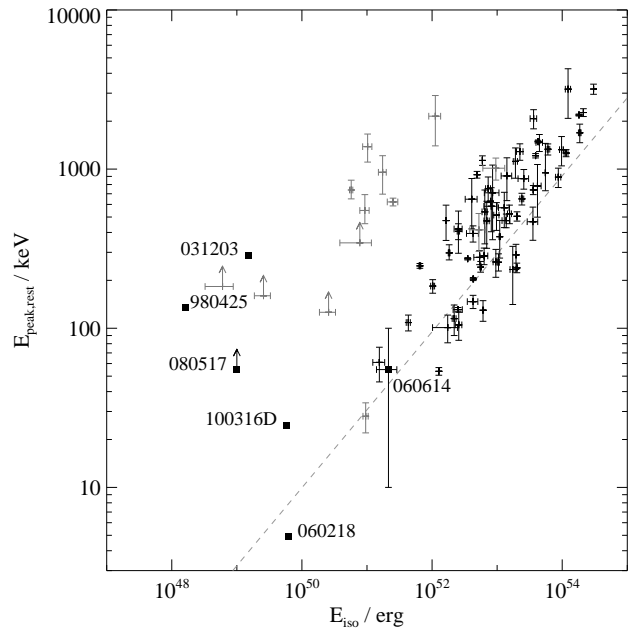


Figure 11. The location of GRB 080517 on the $E_p - E_{iso}$ (Amati) relation, given its redshift of $z = 0.09$. Black points indicate long GRBs, while those in grey are the short GRB population. GRB 080517 and previously identified low luminosity bursts are labelled. The burst lies in an unusual region of parameter space, well below the commonly seen relation for GRBs, placing it in the class of low redshift, low luminosity bursts.

4.2 Afterglow reanalysis

Making use of data analysis tools available from the UK Swift Data Centre², specifying the burst redshift as matching that determined for the host, we have reanalysed the Swift XRT afterglow spectrum and early time series data.

Allowing for absorption at the host redshift only slightly modifies the hydrogen column density required to fit the burst X-ray spectrum observed by *Swift*. The effect on the late time spectrum (mean photon arrival time = $T_0 + 25863$ s, where T_0 is the *Swift* trigger time) is negligible, not modifying the required intrinsic absorption from the $N_H = 6_{-5}^{+4} \times 10^{21} \text{ cm}^{-2}$ in excess of the estimated Galactic absorption estimated with the absorber at $z = 0$ (where the errors on N_H from Swift are 90% confidence rather than 1σ intervals). The early time PC-mode data, with a mean photon arrival of $T_0 + 9559$ s, yields a lower (but consistent) estimated intrinsic absorption ($N_H = 3.4_{-2.0}^{+2.4} \times 10^{21} \text{ cm}^{-2}$), and a photon index of 1.9 ± 0.4 .

Optical/ultraviolet imaging was also obtained by the *Swift*/UVOT instrument, from first acquiring the field to the end of observations at $T_0 + 19$ hrs. Data were observed in 6 bands (*V*, *B*, *U*, *UVW1*, *UVM2* and *UVW2*), and photometric imaging was obtained in each band at intervals throughout this early period. As figure 12 demonstrates, there is little evidence of temporal variation in five of the six bands. Each is consistent with a constant flux. There

² <http://www.swift.ac.uk> (Evans et al. 2009)

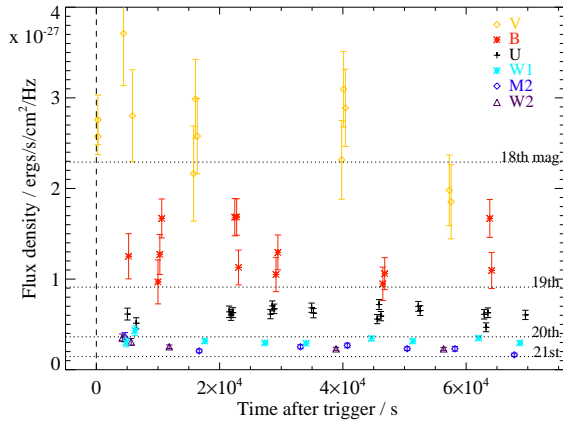


Figure 12. Early time optical and ultraviolet photometry from *Swift*/UVOT. The flux density in the *B* and *U*-band and the three ultraviolet wavebands shows little evidence of variation. There is a hint of declining flux in the *V*-band, but given the large photometric errors in this band, any decline is difficult to constrain with any accuracy.

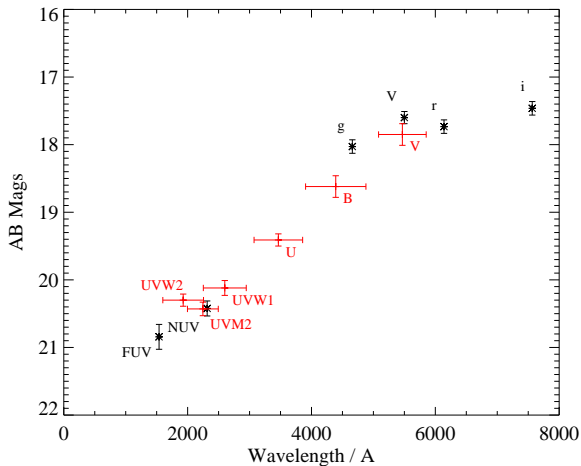


Figure 13. Comparison of averaged early time optical and ultraviolet photometry from *Swift*/UVOT (red, crosses), with the late time observations of the host from other sources (see section 5). The UVOT observations are averaged from T0+0hr to T0+19hr. The late time observations are taken at several years post-burst. Nonetheless, the UVOT observations are consistent (within the photometric errors) with the host galaxy data, suggesting that any afterglow was below the UVOT detection limit.

is a hint of declining flux in the last observations taken in the reddest, *V*, band but the substantial uncertainties on this data preclude a firm identification of afterglow flux. No other band shows a comparable decline during the observation interval.

In figure 13, we compare this early time UVOT data, now integrated across the 19 hour observation assuming no temporal variation, with the late time host galaxy data described in sections 3.1 and 5. While observations in *U* and *B* are not available at late times, the measured flux in the

early time integrated *V* band and near-ultraviolet bands are consistent with that in late time observations of the host galaxy. With the exception of possible variation the *V*-band data, no afterglow is detected within the photometric errors, suggesting that any optical supernova was at or below the UVOT detection limit. Taking the 1σ upper limit on the early time photometry, and subtracting off the late time galaxy flux (see below), we constrain the optical afterglow to $F_\lambda < 2 \times 10^{-17} \text{ ergs s}^{-1} \text{ Å}^{-1}$ at T0+4000s, measured at 5500Å. The *Swift* detected X-ray flux at the same epoch (T0 \sim 5227 $^{+1471}_{-1016}$ s), was $(3.1 \pm 0.8) \times 10^{-13} \text{ ergs s}^{-1} \text{ cm}^{-2}$ in the 0.3-10 keV band. Comparing these yields a limit on X-ray to optical ratio, $\beta_{OX} < 1.0$.

Finally, we have reexamined the early time data from the Liverpool Telescope (LT) observations. Smith et al (2008, GCN 7743) reported limits for non-detection of an optical transient, based on the assumption that it was not coincident with the known source. LT observations commenced at 21:34:05 UT, 674s after the burst trigger. The data comprised imaging of the field in SDSS-*r'*, *i'* and *z'* bands, with 120s individual exposures, the last of which ended at T0+2290s. We confirm that there is no evidence for an early-time excess due to afterglow flux in this source, either in subtractions against our late-time WHT imaging or in pairwise subtraction of early-time exposures. These data provide a relatively weak constraint, but at an early time, enabling us to limit the flux at T0+900s to $F_\lambda < 2 \times 10^{-16} \text{ ergs s}^{-1} \text{ Å}$ at 7500Å. Comparing to the *Swift*-detected X-ray flux at the same epoch, we determine an identical limit to that from the *Swift* optical data alone – $\beta_{OX} < 1.0$.

These limits are formally too weak to satisfy the β_{OX} criterion that is applied to select dark bursts (Jakobsson et al. 2004; van der Horst et al. 2009). Thus the non-detection of the afterglow is consistent with either ‘dark’ or ‘normal’ interpretation. However, we note that this burst shows the high column and red, dusty host more common amongst the dark population (e.g. Hunt et al. 2014; Perley et al. 2013).

Additional *V*-band time series data for this target exists in the second data release of the Catalina Real-time Transient Survey (CRTS, Drake et al. 2009). Both the GRB host and neighbour are well detected. Unfortunately the burst itself occurred during a hiatus in CRTS observing, with no data available until 140 days after the GRB trigger (likely due to Sun avoidance). However, as figure 14 demonstrates, the time series data of the GRB host shows no strong evidence for variability (although a few photometric points are outliers), and allows a precise measurement of the optical magnitude of the host galaxy, $V_{AB} = 17.60 \pm 0.08$. We also investigate the late time optical afterglow, and find no statistically significant evidence for an excess over the host galaxy flux at T+160 days.

5 THE SPECTRAL ENERGY DISTRIBUTION

Our WHT optical imaging in the SDSS *g*, *r*, and *i* bands (described in section 3.1) is supplemented by extensive archival data on these relatively bright sources.

In addition to the *V*-band data from the Catalina Real-time Transient Survey described in section 4.2, we compile archival data in the ultraviolet from the *GALEX* (GR6,

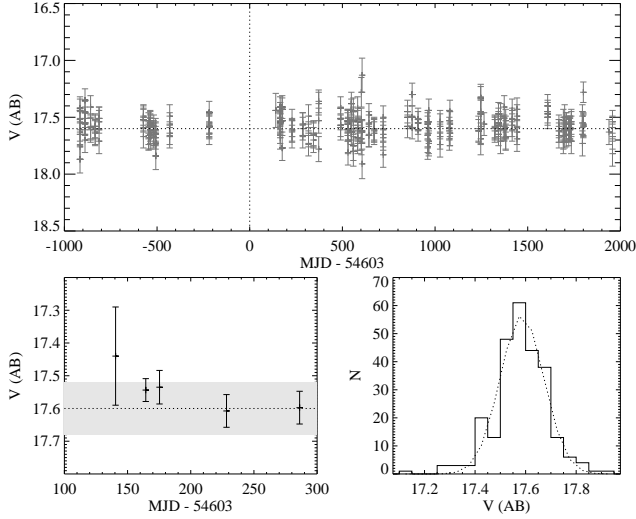


Figure 14. Optical time-series data from the Catalina Real-time Transient Survey for the host galaxy of GRB 0801517. There is no evidence for strong variability in the host galaxy, allowing the time series data to be combined to determine a precise magnitude for the object. In the lower left panel we consider the data closest to the burst data (MJD=54603) in detail, averaging the data points on each night on which the host was observed. While the first three data points lie above the mean measured magnitude, they are within one standard deviation of the time-series mean (shown with shaded region).

Martin et al. 2003) survey and in the near-infrared from the Two Micron All-Sky Survey (2MASS, Skrutskie et al. 2006) as well as the *Wide-Field Infrared Survey Explorer* (WISE, Wright et al. 2010). Both the GRB host and its merging neighbour are detected in the majority of bands from the near-ultraviolet (NUV, $0.15\mu\text{m}$) through to the mid-infrared (W4, $22\mu\text{m}$). While flux from the neighbour is clearly dominated by two principle components in our WHT imaging, these are blended in the remaining data, and we do not attempt to gauge the relative contribution of the two components. Photometry was measured on the images at the source locations, and checked against catalog magnitudes where these were available.

For the W3 and W4 bands (at 12 and $22\mu\text{m}$) where the host and its neighbour are blended in the imaging data, we use magnitudes derived from the ‘ALLWISE’ catalogue values (corrected to AB magnitudes) rather than attempting an independent deblending of the two sources. As noted in the introduction, it is the exceptional brightness of this target in the W3 and W4 bands that initially motivated the follow-up observations described here. While the sources are blended in the W4 band, the light distribution of the host galaxy is distorted, such that it is likely that both the GRB host galaxy and its near neighbour are luminous at $22\mu\text{m}$.

The multi-wavelength photometry of both the GRB host and its neighbour are given in table 2 and figure 15 presents snapshots of the host and neighbour in imaging across the full wavelength range. At $z = 0.09$, the g -band absolute magnitude is $M_g = -20.12 \pm 0.05$ (comparable to that of the Milky Way).

We fit the spectral energy distribution (SED) of the host galaxy using a template fitting approach, minimising

Band	$\lambda_{\text{cen}} / \text{\AA}$	Source	GRB Host	Neighbour
<i>FUV</i>	1540	GALEX	20.84 ± 0.20	20.92 ± 0.22
<i>NUV</i>	2316	GALEX	20.42 ± 0.11	20.74 ± 0.16
<i>g</i>	4660	This work	18.03 ± 0.05	18.42 ± 0.06
<i>V</i>	5500	CRTS	17.60 ± 0.09	18.14 ± 0.12
<i>r</i>	6140	This work	17.73 ± 0.02	18.18 ± 0.05
<i>i</i>	7565	This work	17.46 ± 0.01	18.22 ± 0.02
<i>J</i>	12400	2MASS	17.37 ± 0.13	17.91 ± 0.21
<i>H</i>	16600	2MASS	17.22 ± 0.15	19.56 ± 0.95
<i>Ks</i>	21600	2MASS	17.50 ± 0.20	17.91 ± 0.26
<i>W1</i>	33500	WISE	17.33 ± 0.04	18.49 ± 0.05
<i>W2</i>	46000	WISE	17.57 ± 0.05	19.05 ± 0.12
<i>W3</i>	120000	WISE	15.09 ± 0.05	17.12 ± 0.32
<i>W4</i>	220000	WISE	13.68 ± 0.11	14.78 ± 0.23
Radio	6cm	WSRT	$0.22 \pm 0.04 \text{ mJy}$	

Table 2. Observed photometry measured from broadband observations of the GRB host and its neighbouring galaxy. All magnitudes are given in the AB system. Note that the neighbouring galaxy is undetected in the 2MASS *H*-band and barely detected in *Ks*. Radio fluxes are described in section 3.3. In the 12 and $22\mu\text{m}$ bands we make use of WISE catalog data rather than attempting to deblend the two sources independently.

the χ^2 parameter to determine the best fit age, mass, star formation history and dust extinction. While we could constrain the dust parameter using the extinction derived from the hydrogen Balmer lines, we allow it to vary, recognising that regions contributing to the continuum flux at long wavelengths and those contributing nebular emission flux in the optical may well differ in their extinction properties.

We use as templates the Binary Population and Spectral Synthesis (BPASS) stellar population models of Eldridge & Stanway (2012, 2009) which include a prescription for the nebular emission excited by the stellar continuum. The BPASS models consider the instantaneous-burst and constant star formation rate cases. In both cases, we modify the templates using the Calzetti et al. (2000) dust extinction law. This was derived for local infrared-luminous galaxies with active star formation, and would appear appropriate in this case, given the bright infrared fluxes measured.

The photometry shows a challenging combination of a very flat optical spectrum (which implies little extinction and potentially even a non-stellar continuum) and evidence for strong dust emission in the infrared (see figure 16). The BPASS population synthesis models include a treatment of stellar evolution pathways through binary evolution. For young stellar populations, this treatment results in a relatively blue UV-optical continuum at a given age (and hence larger energy budget for heating dust) compared to models which neglect such pathways. To model the re-emission of thermal photons at longer wavelengths, we adopt the energy-balance prescription of da Cunha, Charlot, & Elbaz (2008), and re-emit the energy lost from the UV-optical as a combination of black body and PAH emission components. For the latter we scale the composite mid-infrared spectrum determined for star forming galaxies by Smith et al. (2007). The W3 and W4 bands were excluded from the fitting procedure, in order to assess whether the observed UV-optical continuum were able to correctly predict the mid-infrared flux, or whether an additional, heavily dust-extincted component was required.

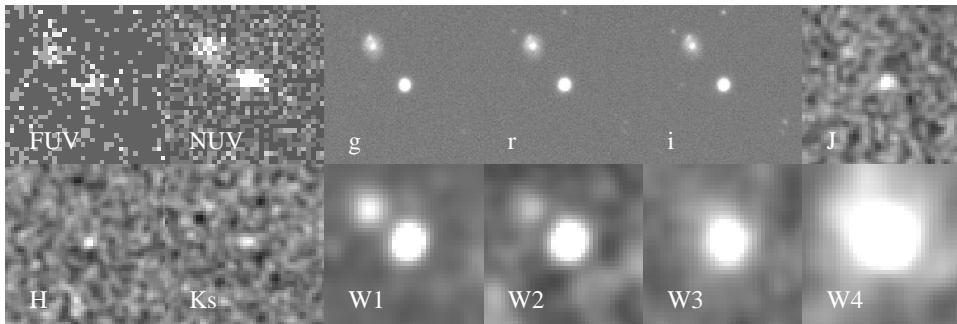


Figure 15. Snapshot images of the host-neighbour system from the ultraviolet through to the infrared. Boxes are 50 arcseconds on a side, centred on the GRB host, and oriented with North up and East to the left. Note the exceptionally red colours of both sources, but particularly the GRB host, in the WISE (infrared) bands.

The best fitting single SED model to the host photometry is not one dominated by nebular emission or continuous star formation, but rather a post-starburst template, observed 500 Myr after the initial starburst, as shown in figure 16. The derived stellar mass is $\log_{10}(M_*/M_\odot) = 9.58^{+0.12}_{-0.16}$, and a relatively low extinction of $A_V = 0.16 \pm 0.02$ is required for the dominant stellar component. This model reproduces the GRB host galaxy’s ultraviolet and infrared continua, while underestimating its optical flux by $\sim 25 - 50\%$. We note that fitting instead with the (Maraston 2005) stellar population synthesis models returns similar parameters, albeit with a relatively poor fit to the data. The mass, low extinction and age of the dominant stellar component imply that, for $z = 0.09$, the GRB host represents a relatively young, slightly sub- L^* galaxy.

As section 3.2 demonstrated, there is a substantial contribution to the optical from line emission, which may account for some part of this discrepancy. In the r -band in particular, line emission likely contributes a minimum of 12% of the broadband flux. To address this, we also allow an additional component of continuous ongoing star formation with moderate dust extinction (as seen in the Balmer series), while cautioning that this may be overfitting the limited data. We find that the star forming component required for the best fit combination contributes a mere 0.1% of the stellar mass of the system. Including such a component improves the fit in the optical and at 12 and $22\mu\text{m}$, but causes the flux in the K_S band and $4.6\mu\text{m}$ W2 band to be somewhat overestimated (again, by a factor of $\sim 50\%$). Since the latter lies at the transition between the stellar and dust components of the template, it is possible that this transition is not correctly addressed in the modelling, and potentially that a steeper spectral index is required in the infrared PAH emission region than is seen in the IR-luminous galaxy composite used (Smith et al. 2007).

Explanations for the comparatively low flux measured in the 2MASS K_S band, and the non-detection of the neighbour in the H -band (see figure 15), are less clear. It is likely that deeper near-infrared photometry is required to address this issue. We note that the stellar population templates fail to entirely reproduce the high fluxes seen in the $22\mu\text{m}$ W4 band, implying that at least some fraction of the stellar emission in this system is heavily extinguished and undetectable in the UV-optical. Further observations at millime-

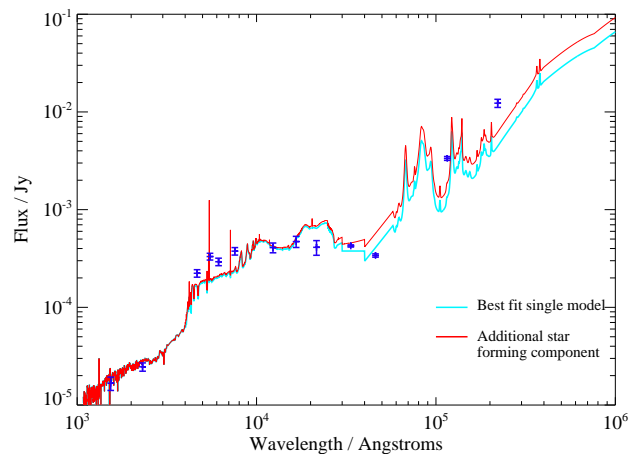


Figure 16. The best fitting model templates to the host galaxy photometry. The pale cyan line indicates the best fitting single template: a mature system observed 0.5 Gyr after an initial starburst. In red we show the best fit derived when a component of ongoing star formation (at age 1 Myr, contributing just 0.1% of the stellar mass) is allowed in addition to the dominant model.

tre/submillimetre wavelengths will also be required to properly constrain this emission region.

6 STAR FORMATION IN THE HOST OF GRB 080517

The host of GRB 080517 is an actively star forming galaxy at $z = 0.09$. The evidence for ongoing star formation is overwhelming, based on the presence of i) strong $H\alpha$ (and other Balmer) emission lines, ii) GALEX FUV and NUV flux, iii) $22\mu\text{m}$ emission and iv) a 4.8 GHz radio detection, not to mention the initial selection through detection of a core-collapse gamma-ray burst.

In table 3 we compare the star formation rates (SFRs) derived from these different proxies. In all cases, the star formation rate conversion used is subject to significant systematic uncertainty, but those at $0-22\mu\text{m}$ are derived primarily for young (< 100 Myr) stellar populations with continuous star formation, while that for the radio continuum is based

primarily on resolved measurements of nearby star forming galaxies. No attempt is made to correct for dust extinction, which may well be affecting different indicators differently, and so these values are effectively lower limits on the total star formation rate.

Unsurprisingly, the near-ultraviolet continuum (which is most affected by the presence of dust extinction) gives the lowest estimate of $0.43 \pm 0.07 \text{ M}_\odot \text{ yr}^{-1}$. In the Calzetti et al. (2000) extinction paradigm, the continuum is subject to 0.44 times the extinction in the nebular component, or $E(B - V) = 0.53$. This corresponds to a measured 2300Å flux only 2% of its intrinsic value. In fact, the emission in the GALEX band appears to be associated with the mature stellar population (see section 5) rather than the heavily-extincted star forming component.

The star formation rates derived from the optical H α emission line and the 22 μm continuum (measured in the W4 band) are consistent at the 1σ level, each estimating rates around $16 \text{ M}_\odot \text{ yr}^{-1}$. Interestingly, this may suggest that the 1.5 arcsecond wide slit used for spectroscopy may have captured the majority of the flux from active star formation in the GRB host galaxy, despite its relatively large (~ 2 arcsecond full-width at half-maximum) light distribution.

Curiously, the final star formation rate indicator, that derived from the radio continuum at 4.5 GHz produces a relatively low estimate at $7.6 \pm 1.4 \text{ M}_\odot \text{ yr}^{-1}$, only about half that determined from the previous two measures, using the conversion rate determined by Murphy et al. (2011), and extrapolating to 1.4 GHz using a radio spectral slope $\alpha = 0.75$. An alternate conversion factor (Yun & Carilli 2002) yields a similar but still lower estimate ($4 \text{ M}_\odot \text{ yr}^{-1}$).

The synthesised beam of the WSRT at 4.8 GHz is insufficient to have resolved out a significant fraction of the flux in this source, and the flux density is measured at better than 5σ , making it likely that this is a genuine decrement. Gigahertz frequency radio continuum in star forming galaxies arises primarily from non-thermal synchrotron emission, generated by the electrons accelerated by supernovae and their remnants. This introduces a time delay between the onset of star formation and the establishment of a radio continuum, the length of which will depend on the mass distribution, metallicity and other properties of the stellar population. As a result, the radio continuum flux density associated with ongoing star formation rises rapidly with age of the star forming population before stabilising at $> 100 \text{ Myr}$ (Bressan, Silva, & Granato 2002). If, then, the young 1 Myr starburst suggested by the BPASS models presents a true picture of the ongoing star formation in this source, it is possible that a strong radio continuum has yet to become established and a radio flux - SFR conversion factor up to an order of magnitude higher might be appropriate. Future observations at further radio/submillimeter frequencies, and a measurement of the radio spectral slope, may help to constrain the effect of star formation history on this estimate.

7 THE HOST AND ENVIRONMENT OF GRB 080517

The host of GRB 080517 appears to be a compact, smooth galaxy in the local Universe. Given its UV-optical photom-

Proxy	SFR/ $\text{M}_\odot \text{ yr}^{-1}$	Conversion factor
NUV continuum	0.43 ± 0.07	Hao et al. (2011)
H α line emission	15.5 ± 0.4	Hao et al. (2011)
22 μm continuum	16.5 ± 1.5	Lee et al (2013)
4.8 GHz continuum	7.6 ± 1.4	Murphy et al. (2011)

Table 3. Star formation rates derived from different proxies observed for the host of GRB 080517. In the radio we apply the conversion factor derived at 1.4 GHz, assuming a radio spectral slope of 0.75.

etry, there would be little reason to expect significant ongoing star formation. Nonetheless, as the previous section describes, there is substantial evidence for an ongoing, young and fairly dusty (based on H α /H β) starburst, which likely dominates emission at $> 10 \mu\text{m}$.

In this context, the presence of a near neighbour (separated by only $\sim 25 \text{ kpc}$ at $z = 0.09$) is intriguing. The two galaxies have comparable masses (the neighbour is just ~ 0.5 magnitudes fainter than the GRB host and similar in colour), and any interaction between them will constitute a major incident in the history of both galaxies. The gravitational forces caused by a near fly-by in the recent past could well have been sufficient to trigger the starburst detected in both sources - a starburst somewhat obscured by dust. It is also notable that the cores of both galaxies (including both components of the neighbour) and the GRB X-ray error circle lie along a common axis. Further modelling of the dynamics of this system, supported by integral field spectroscopy, and a search for low surface-brightness distortions in the morphology of both galaxies, will be necessary to confirm this picture, but the existing evidence is suggestive.

Long-duration GRBs are typically associated with the peak light in their host galaxies, and with recent star formation (e.g Svensson et al. 2010). However, the broadband continuum emission of the host of GRB 080517 is dominated by a much older stellar population. If, then, we hypothesise that the GRB is associated with the recent episode of star formation in this system, we are left with the conclusion that it occurred in a dusty region ($E(B - V) = 1.2$) undergoing an intense star burst ($\text{SFR} \sim 16 \text{ M}_\odot \text{ yr}^{-1}$). Such dust extinction is consistent with the excess neutral hydrogen column inferred from the X-ray afterglow, and potentially with the failure of early-time optical observations to identify an optical transient distinguishable from the host galaxy.

As we have already discussed, it is impossible to determine whether GRB 080517 would indeed have met the ‘dark’ burst criterion if deeper observations were available. It is, however, possible to consider whether its host lies in a similar region of parameter space to known dark bursts. Perley et al. (2013) recently presented a systematic analysis of the dark GRB host galaxy population, examining both their afterglow properties and those derived from fitting of the host galaxy spectral energy distribution. As figures 17 and 18 demonstrate, the inferred characteristics of the host of GRB 080517 lie comfortably within the distribution of ‘dark’ burst hosts in terms of afterglow spectral index, hydrogen column density, stellar mass and inferred star formation rate, although the last is higher than those in dark bursts at $z < 0.5$, and more akin to those observed at higher redshifts (Perley et al. 2013).

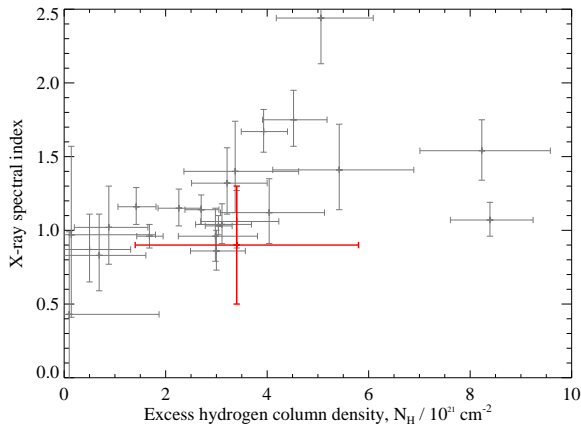


Figure 17. The X-ray afterglow properties of GRB 080517 compared to those of ‘dark’ bursts as given by Perley et al. (2013). GRB 080517 (bold, red symbol) has an afterglow spectral index, and shows an excess neutral hydrogen column density above that in our own Galaxy, which is consistent with those of the dark GRB population, and follows the same correlation.

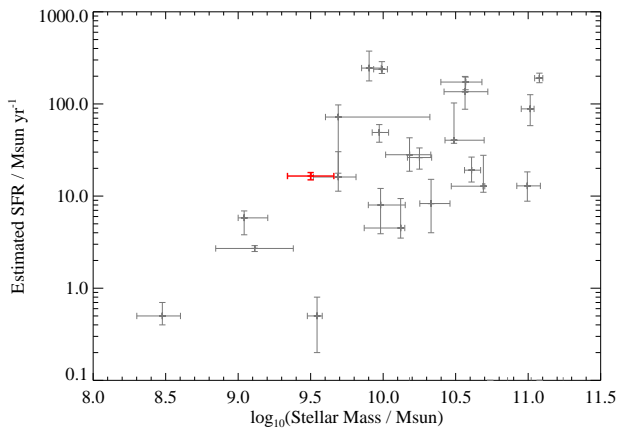


Figure 18. The host mass of GRB 080517, and star formation rate inferred from H α line emission, compared to those of ‘dark’ bursts as given by Perley et al. (2013). GRB 080517 (bold, red symbol) has an inferred stellar mass (based on SED fitting) comparable to those of the dark burst population, and follows the same mass-star formation rate trend.

Whether or not GRB 080517 is indeed a local example of a ‘dark’ host, one advantage it offers is the opportunity to study its optical spectrum in a detail challenging for higher redshift GRB hosts of either dark or normal types.

In figures 19 and 20 we compare its optical emission line ratios to those of local emission-line galaxies from the SDSS (Brinchmann et al. 2004). The GRB host has line ratios consistent with a Solar or slightly super-Solar metallicity, and is within the range of scatter of the SDSS sample, although well above the relationship between the R_{23} and $[O III]/[O II]$ at a given metallicity determined by Maiolino et al. (2008). This is consistent with the results from the less metal-sensitive SED fitting procedure described in section 5, in which 0.5–1.0 Solar metallicity

templates were narrowly preferred over those with significantly lower metal enrichment. While far from unique (e.g. Savaglio et al. 2012; Krühler et al. 2012), this places the host of GRB 080517 towards the upper end of the metallicity distribution for GRB hosts. Interestingly, at least two other high metallicity bursts, GRB 020819 (Levesque et al. 2010) and GRB 080607 (Prochaska et al. 2009), are dark bursts.

The BPT diagram (Baldwin, Phillips, & Terlevich 1981) is an established indicator of starburst versus AGN character, since the different ionisation parameters arising from the two classes have a strong effect on optical emission line ratios and particularly the ratio of $[N II]$ to $H\alpha$. As figure 19 demonstrates, the two components of the neighbouring source are broadly consistent with a star-formation driven spectrum, although both lie above the local mean in $[O III]/H\beta$ (a trait also often seen in high redshift star-forming galaxies, e.g. Masters et al. 2014; Stanway et al. 2014). While component A has measured line ratios consistent with a ‘composite’ spectrum, large errors on the measured values permit a purely star forming spectrum.

The line ratios of the GRB host galaxy are intriguing, placing it too in the region of the parameter space usually described as ‘composite’, suggesting that there might plausibly be a contribution to the ionising spectrum from an AGN. If so, this would be a surprise, since gamma ray bursts have not previously been associated with active galaxies, but may help to explain the excess flux seen in the $22\mu m$ band where a hot AGN would be expected to make a contribution to PAH emission.

Unfortunately *Swift* did not track the burst beyond 20 hours after the trigger, at which point the X-ray afterglow was still fading. However the measured flux at this late epoch provides a firm upper limit on possible X-ray flux from the host galaxy of $4.3^{+2.8}_{-2.0} \times 10^{-14} \text{ ergs cm}^2 \text{ s}^{-1}$ in the *Swift* XRT 0.3–10 keV band. The luminosity of any hypothetical AGN at $z = 0.09$ is therefore constrained to an $L_X < 8.6 \times 10^{41} \text{ ergs s}^{-1}$, placing it at the very low end of the AGN luminosity distribution (e.g. Silverman et al. 2008; Brusa et al. 2010). As noted in section 4.2, there is also little evidence for any optical variability in the host galaxy, either before or after the gamma ray burst, as might be expected of a galaxy with a strong AGN contribution.

While the centre of the host galaxy lies outside the 90% confidence interval on the X-ray location of the GRB (based on the refined XRT analysis), the two locations are consistent at the 2σ uncertainty level. It is therefore not impossible that the gamma-ray burst resulted from activity in the galactic nucleus.

A rare class of gamma ray flares are known to result from a sudden accretion event due to the tidal disruption of stars around supermassive black holes (Bloom et al. 2011; Cenko et al. 2012, Brown et al. submitted). The burst of accretion in such sources launches a relativistic jet, and would result in a short-lived burst of AGN activity from otherwise quiescent galactic nuclei. In this context, the plausible association of GRB 080517 with a very low luminosity AGN at ~ 6 years post burst merits further investigation and monitoring of this system.

Further observations will be required to place firmer constraints on the presence or absence of an AGN at late times and any late time variability. We note that if there is no AGN contribution, then the optical emission line ratios in

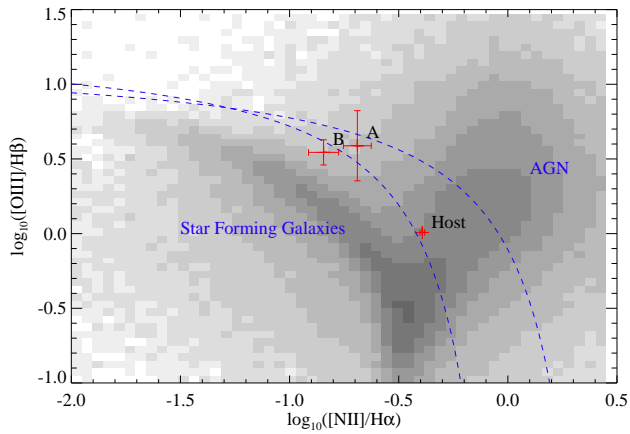


Figure 19. The emission line strengths of the GRB host galaxy and its neighbour (components A and B) placed on the classic BPT diagram. All three sources lie above the locus of star forming galaxies measured in the SDSS, although the neighbour remains consistent with a star forming origin. The dashed lines indicate the classification criteria of Kauffmann et al. (2003). The region between the dashed lines is described as a ‘composite’ region and may indicate contributions from both star formation and AGN activity. The background density plot shows the distribution of galaxies in the SDSS (Brinchmann et al. 2004). Interestingly, the GRB host lies in the ‘composite’ region of the parameter space, suggesting that it may have an AGN component in addition to ongoing star formation.

the host imply star formation with a steep ultraviolet spectrum, causing a higher ionisation parameter than is typical at low redshifts, and perhaps strengthening the suggestion that this is a very young, intense starburst (as suggested by the BPASS stellar population models).

8 CONCLUSIONS

In this paper we have presented an analysis of new and archival data for the host galaxy of GRB 080517. Our main conclusions can be summarised as follows:

- (i) GRB 080517 is a rare, low luminosity, long gamma ray burst.
- (ii) Our WHT spectroscopy reveals that the host galaxy of GRB 080517 is a strong optical line emitter lying at $z = 0.09$.
- (iii) The morphology of the GRB host appears to be smooth and compact with a half light radius, deconvolved with the seeing, of 2.7 kpc. Its light distribution is consistent with a Sersic index of $n = 1.5 \pm 1.0$.
- (iv) The strong optical emission line ratios in the GRB host are consistent with a composite AGN+starburst spectrum at Solar or super-Solar metallicity, and the ratio of Balmer lines suggests the nebular emission is subject to an extinction $E(B - V) = 1.2$.
- (v) The spectral energy distribution of the galaxy in the UV-optical is broadly reproduced by a post-starburst template at an age of 500 Myr, with a relatively small component of ongoing star formation ($< 1\%$ of the stellar mass). However no template considered provides a good match to

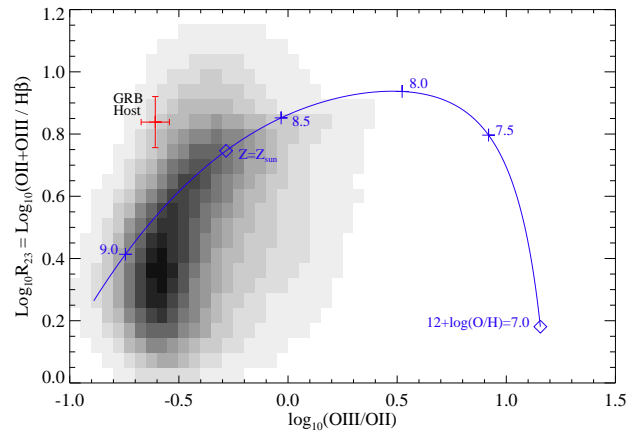


Figure 20. Metallicity-sensitive optical line ratios for the GRB host galaxy. The well known R_{23} index is plotted against the ratio of oxygen lines in order to break the degeneracy in metallicity in the former. The majority of SDSS sources (greyscale) are relatively local and high in metallicity (Brinchmann et al. 2004). The solid line shows the metallicity parameterisation of Maiolino et al. (2008). The GRB host galaxy lies well above the typical SDSS galaxy in R_{23} but within the distribution of local sources. We note that the effects of correcting for differential dust extinction on the lines is to move it further from the SDSS relation. Its measured line ratios are consistent with a slightly super-Solar metallicity.

all features of the SED, and in particular to the high fluxes measured at $> 10\mu\text{m}$, suggesting that multiple components with different spectral energy distributions may contribute to the broadband flux.

- (vi) Star formation rate estimates for the GRB host range from $0.43 M_{\odot} \text{ yr}^{-1}$ to $16.5 M_{\odot} \text{ yr}^{-1}$, based on different indicators. The low rate estimated from the ultraviolet continuum likely arises due to strong dust extinction in the star forming regions. Estimates from the $H\alpha$ line and $22\mu\text{m}$ are consistent at 15.5 ± 0.4 and $16.5 \pm 1.5 M_{\odot} \text{ yr}^{-1}$.

- (vii) We detect radio emission from the host galaxy with a flux density, $S_{4.8 \text{ GHz}} = 0.22 \pm 0.04 \text{ mJy}$. This corresponds to a star formation rate of $7.6 \pm 1.4 M_{\odot} \text{ yr}^{-1}$.

- (viii) The high ionisation parameter seen in the optical line ratios, low radio flux and SED fitting are all consistent with a very young ($< 100 \text{ Myr}$) star formation episode.

- (ix) The host galaxy has a close companion within 25 kpc in projected distance and lying at the same redshift. The companion shows distorted morphology, including two cores which appear to be undergoing a merger. The proximity of these galaxies may indicate that the GRB progenitor formed in an ongoing starburst triggered by gravitational interaction.

- (x) While the burst afterglow was too faint to tightly constrain the X-ray to optical flux ratio, its properties and those of its host galaxy are consistent with those of the ‘dark’ GRB population. The host galaxy’s properties and wider environment suggest that the role of galaxy-galaxy interaction in triggering bursts in relatively massive, metal rich galaxies needs to be considered more carefully.

We aim to investigate this field further, obtaining stronger X-ray constraints on the presence of AGN activity,

high resolution imaging, and also further radio continuum measurements of the host's dust-obscured star formation.

ACKNOWLEDGMENTS

We thank the anonymous referee of this paper for helpful comments and suggestions. ERS and AJL acknowledge funding from the UK Science and Technology Facilities Council under the Warwick Astrophysics consolidated grant ST/L000733/1. ERS thanks Dr Elmé Breedt for useful discussions and recommending the CRTS. AJvdH acknowledges the support of the European Research Council Advanced Investigator Grant no. 247295 (PI: R.A.M.J. Wijers). CGM acknowledges support from the Royal Society, the Wolfson Foundation and STFC.

Optical data were obtained from the William Herschel Telescope. The WHT and its override programme are operated on the island of La Palma by the Isaac Newton Group in the Spanish Observatorio del Roque de los Muchachos of the Instituto de Astrofísica de Canarias. We also make use of data from the Liverpool Telescope which is operated on the island of La Palma by Liverpool John Moores University in the Spanish Observatorio del Roque de los Muchachos of the Instituto de Astrofísica de Canarias with financial support from the UK Science and Technology Facilities Council.

Radio data were obtained from WSRT. The WSRT is operated by ASTRON (Netherlands Institute for Radio Astronomy) with support from the Netherlands foundation for Scientific Research. This work made use of data supplied by the UK Swift Science Data Centre at the University of Leicester (Evans et al. 2009). We also made use of Ned Wright's very useful cosmology calculator (Wright 2006).

Based in part on public data from GALEX GR6. The Galaxy Evolution Explorer (GALEX) satellite is a NASA mission led by the California Institute of Technology. This publication also makes use of data products from the Wide-field Infrared Survey Explorer, which is a joint project of the University of California, Los Angeles, and the Jet Propulsion Laboratory/California Institute of Technology, funded by the National Aeronautics and Space Administration. This publication further makes use of data products from the Two Micron All Sky Survey, which is a joint project of the University of Massachusetts and the Infrared Processing and Analysis Center/California Institute of Technology, funded by the National Aeronautics and Space Administration and the National Science Foundation.

Data is also derived from the Catalina Real-time Transient Survey. The CSS survey is funded by the National Aeronautics and Space Administration under Grant No. NNG05GF22G issued through the Science Mission Directorate Near-Earth Objects Observations Program. The CRTS survey is supported by the U.S. National Science Foundation under grants AST-0909182 and AST-1313422.

We make use of SDSS-III data. Funding for SDSS-III has been provided by the Alfred P. Sloan Foundation, the Participating Institutions, the National Science Foundation, and the U.S. Department of Energy Office of Science. The SDSS-III web site is <http://www.sdss3.org/>.

SDSS-III is managed by the Astrophysical Research Consortium for the Participating Institutions of the SDSS-III Collaboration including the University of Arizona, the

Brazilian Participation Group, Brookhaven National Laboratory, Carnegie Mellon University, University of Florida, the French Participation Group, the German Participation Group, Harvard University, the Instituto de Astrofísica de Canarias, the Michigan State/Notre Dame/JINA Participation Group, Johns Hopkins University, Lawrence Berkeley National Laboratory, Max Planck Institute for Astrophysics, Max Planck Institute for Extraterrestrial Physics, New Mexico State University, New York University, Ohio State University, Pennsylvania State University, University of Portsmouth, Princeton University, the Spanish Participation Group, University of Tokyo, University of Utah, Vanderbilt University, University of Virginia, University of Washington, and Yale University.

REFERENCES

- Ahn C. P., et al., 2014, *ApJS*, 211, 17
- Amati L., et al., 2002, *A&A*, 390, 81
- Amati L., 2006, *MNRAS*, 372, 233
- Baldwin J. A., Phillips M. M., Terlevich R., 1981, *PASP*, 93, 5
- Berger E., Cowie L. L., Kulkarni S. R., Frail D. A., Ausserl H., Barger A. J., 2003, *ApJ*, 588, 99
- Bloom J. S., et al., 2011, *Sci*, 333, 203
- Bressan A., Silva L., Granato G. L., 2002, *A&A*, 392, 377
- Brinchmann J., Charlot S., White S. D. M., Tremonti C., Kauffmann G., Heckman T., Brinkmann J., 2004, *MNRAS*, 351, 1151
- Brusa M., et al., 2010, *ApJ*, 716, 348
- Butler N. R., Kocevski D., 2007, *ApJ*, 663, 407
- Calzetti D., Armus L., Bohlin R. C., Kinney A. L., Koornneef J., Storchi-Bergmann T., 2000, *ApJ*, 533, 682
- Campana S., et al., 2006, *Nature*, 442, 1008
- Cano Z., et al., 2011, *ApJ*, 740, 41
- Castro Cerón J. M., Michałowski M. J., Hjorth J., Malesani D., Gorosabel J., Watson D., Fynbo J. P. U., Morales Calderón M., 2010, *ApJ*, 721, 1919
- Cenko S. B., et al., 2012, *ApJ*, 753, 77
- Cenko S. B., et al., 2009, *ApJ*, 693, 1484
- Chapman R., Tanvir N. R., Priddey R. S., Levan A. J., 2007, *MNRAS*, 382, L21
- Chen H.-W., et al., 2009, *ApJ*, 691, 152
- Christensen L., Hjorth J., Gorosabel J., 2004, *A&A*, 425, 913
- da Cunha E., Charlot S., Elbaz D., 2008, *MNRAS*, 388, 1595
- Della Valle M., et al., 2006, *Nature*, 444, 1050
- Drake A. J., et al., 2009, *ApJ*, 696, 870
- Eldridge J. J., Stanway E. R., 2012, *MNRAS*, 419, 479
- Eldridge J. J., Stanway E. R., 2009, *MNRAS*, 400, 1019
- Ellison S. L., Patton D. R., Simard L., McConnachie A. W., 2008, *AJ*, 135, 1877
- Evans P. A., et al., 2009, *MNRAS*, 397, 1177
- Evans P. A., Goad M. R., Osborne J. P., Beardmore A. P., 2008, *GCN*, 7744, 1
- Fenimore E. E., Madras C. D., Nayakshin S., 1996, *ApJ*, 473, 998
- Fishman G. J., 1995, *PASP*, 107, 1145
- Fruchter A. S., et al., 2006, *Nature*, 441, 463
- Fynbo J. P. U., et al., 2009, *ApJS*, 185, 526

- Fynbo J. P. U., et al., 2006, *Nature*, 444, 1047
- Galama T. J., et al., 1998, *Nature*, 395, 670
- Gal-Yam A., et al., 2006, *Nature*, 444, 1053
- Gehrels N., et al., 2006, *Nature*, 444, 1044
- Gehrels N., et al., 2004, *ApJ*, 611, 1005
- Giallisco M., et al., 2004, *ApJ*, 600, L93
- Graham A. W., Driver S. P., 2005, *PASA*, 22, 118
- Graham J. F., Fruchter A. S., 2013, *ApJ*, 774, 119
- Greiner J., et al., 2011, *A&A*, 526, A30
- Greiner J., et al., 2013, *A&A*, 560, A70
- Hatsukade B., Hashimoto T., Ohta K., Nakanishi K., Tamura Y., Kohno K., 2012, *ApJ*, 748, 108
- Hao J.-M., Yuan Y.-F., 2013, *ApJ*, 772, 42
- Hao C.-N., Kennicutt R. C., Johnson B. D., Calzetti D., Dale D. A., Moustakas J., 2011, *ApJ*, 741, 124
- Hjorth J., et al., 2012, *ApJ*, 756, 187
- Hunt L. K., et al., 2014, *arXiv*, arXiv:1402.4006
- Jakobsson P., et al., 2012, *ApJ*, 752, 62
- Jakobsson P., Hjorth J., Fynbo J. P. U., Watson D., Pedersen K., Björnsson G., Gorosabel J., 2004, *ApJ*, 617, L21
- Kamble A., Soderberg A., Berger E., Zauderer A., Chakraborti S., Williams P., 2014, *arXiv*, arXiv:1401.1221
- Kaneko Y., et al., 2007, *ApJ*, 654, 385
- Kann D. A., et al., 2010, *ApJ*, 720, 1513
- Kauffmann G., et al., 2003, *MNRAS*, 346, 1055
- Kocevski D., Butler N., 2008, *ApJ*, 680, 531
- Kohno K., et al., 2005, *PASJ*, 57, 147
- Kouveliotou C., Meegan C. A., Fishman G. J., Bhat N. P., Briggs M. S., Koshut T. M., Paciesas W. S., Pendleton G. N., 1993, *ApJ*, 413, L101
- Krühler T., et al., 2011, *A&A*, 534, A108
- Krühler T., et al., 2012, *arXiv*, arXiv:1205.4036
- Krühler T., et al., 2012, *A&A*, 546, A8
- Lee J. C., Hwang H. S., Ko J., 2013, *ApJ*, 774, 62
- Levesque E. M., Kewley L. J., Berger E., Zahid H. J., 2010, *AJ*, 140, 1557
- Levesque E. M., Kewley L. J., Graham J. F., Fruchter A. S., 2010, *ApJ*, 712, L26
- Madau P., Haardt F., Rees M. J., 1999, *ApJ*, 514, 648
- Mainzer A., et al., 2011, *ApJ*, 731, 53
- Maiolino R., et al., 2008, *A&A*, 488, 463
- Malesani D., et al., 2004, *ApJ*, 609, L5
- Maraston C., 2005, *MNRAS*, 362, 799
- Markwardt C., et al., 2008, *GCN*, 7748, 1
- Martin C., et al., 2003, *SPIE*, 4854, 336
- Masters D., et al., 2014, *ApJ*, 785, 153
- Melandri A., et al., 2012, *MNRAS*, 421, 1265
- Michałowski M. J., et al., 2014, *A&A*, 562, A70
- Michałowski M. J., et al., 2012, *ApJ*, 755, 85
- Michałowski M. J., et al., 2009, *ApJ*, 693, 347
- Miller N. A., Fomalont E. B., Kellermann K. I., Mainieri V., Norman C., Padovani P., Rosati P., Tozzi P., 2008, *ApJS*, 179, 114
- Moin A., et al., 2013, *ApJ*, 779, 105
- Morrison G. E., Owen F. N., Dickinson M., Ivison R. J., Ibar E., 2010, *ApJS*, 188, 178
- Murphy E. J., et al., 2011, *ApJ*, 737, 67
- Nakagawa Y. E., et al., 2006, *PASJ*, 58, L35
- Nousek J. A., et al., 2006, *ApJ*, 642, 389
- Oke J. B., Gunn J. E., 1983, *ApJ*, 266, 713
- Osterbrock D. E., Ferland G. J., 2006, 'The Astrophysics of Gaseous Nebulae and AGN', 2nd Edition, University Science Books, Sausalito CA.
- Parsons A. M., et al., 2008, *GCN*, 7742, 1
- Patton D. R., Carlberg R. G., Marzke R. O., Pritchet C. J., da Costa L. N., Pellegrini P. S., 2000, *ApJ*, 536, 153
- Pellizza L. J., et al., 2006, *A&A*, 459, L5
- Perley D. A., et al., 2014, *arXiv*, arXiv:1407.4456
- Perley D. A., et al., 2013, *ApJ*, 778, 128
- Perley D. A., Perley R. A., 2013, *ApJ*, 778, 172
- Pian E., et al., 2006, *Nature*, 442, 1011
- Priddey R. S. et al., 2006, *MNRAS*, 369, 1189
- Prochaska J. X., et al., 2009, *ApJ*, 691, L27
- Robertson B. E., Ellis R. S., 2012, *ApJ*, 744, 95
- Rol E., Wijers R. A. M. J., Kouveliotou C., Kaper L., Kaneko Y., 2005, *ApJ*, 624, 868
- Salvaterra R., et al., 2012, *ApJ*, 749, 68
- Sault, R. J., Teuben, P. J., & Wright, M. C. H. 1995, *Astronomical Data Analysis Software and Systems IV*, 77, 433
- Savaglio S., Glazebrook K., LeBorgne D., 2009, *ApJ*, 691, 182
- Savaglio S., et al., 2012, *MNRAS*, 420, 627
- Sazonov S. Y., Lutovinov A. A., Sunyaev R. A., 2004, *Nature*, 430, 646
- Schlafly E. F., Finkbeiner D. P., 2011, *ApJ*, 737, 103
- Skrutskie M. F., et al., 2006, *AJ*, 131, 1163
- Silverman J. D., et al., 2008, *ApJ*, 679, 118
- Smith R. J., et al., 2008, *GCN*, 7743, 1
- Smith J. D. T., et al., 2007, *ApJ*, 656, 770
- Soderberg A. M., et al., 2004, *Nature*, 430, 648
- Stanway E. R., Davies L. J. M., Levan A. J., 2010, *MNRAS*, 409, L74
- Stanway E. R., Bremer M. N., Tanvir N. R., Levan A. J., Davies L. J. M., 2011, *MNRAS*, 410, 1496
- Stanway E. R., Levan A. J., Davies L. J. M., 2014, *MNRAS*, 444, 2133
- Stanway E. R., Eldridge J. J., Greis S. M. L., Davies L. J. M., Wilkins S. M., Bremer M. N., 2014, *arXiv*, arXiv:1408.4122
- Starling R. L. C., et al., 2011, *MNRAS*, 411, 2792
- Svensson K. M., Levan A. J., Tanvir N. R., Fruchter A. S., Strolger L.-G., 2010, *MNRAS*, 479
- Symeonidis M., et al., 2014, *arXiv*, arXiv:1406.2599
- Tanvir N. R., et al., 2004, *MNRAS*, 352, 1073
- Tan, G. H. 1991, *IAU Colloq. 131: Radio Interferometry. Theory, Techniques, and Applications*, 19, 42
- Tanvir N. R., Levan A. J., Fruchter A. S., Hjorth J., Hounsell R. A., Wiersema K., Tunnicliffe R. L., 2013, *Nature*, 500, 547
- Tanvir N. R., et al., 2012, *ApJ*, 754, 46
- Thoenes C. C., Perley D. A., Bloom J. S., 2007, *GCN*, 6663, 1
- van der Horst A. J., Kouveliotou C., Gehrels N., Rol E., Wijers R. A. M. J., Cannizzo J. K., Racusin J., Burrows D. N., 2009, *ApJ*, 699, 1087
- Vaughan S., et al., 2004, *ApJ*, 603, L5
- Weiler K. W., Panagia N., Montes M. J., Sramek R. A., 2002, *ARA&A*, 40, 387
- Watson D., et al., 2011, *ApJ*, 741, 58
- Watson D., et al., 2006, *ApJ*, 636, 967
- Watson D., et al., 2004, *ApJ*, 605, L101
- Wiersema K., 2011, *MNRAS*, 414, 2793
- Woosley S. E., Heger A., 2006, *ApJ*, 637, 914

Wright E. L., 2006, *PASP*, 118, 1711
Wright E. L., et al., 2010, *AJ*, 140, 1868
Xiao L., Schaefer B. E., 2011, *ApJ*, 731, 103
Yun M. S., Carilli C. L., 2002, *ApJ*, 568, 88
Zauderer B. A., et al., 2013, *ApJ*, 767, 161

This paper has been typeset from a $\mathrm{T}_{\mathrm{E}}\mathrm{X}/\mathrm{L}^{\mathrm{A}}\mathrm{T}_{\mathrm{E}}\mathrm{X}$ file prepared by the author.